Ranking of Different Wavelets in the Computation of Phase-Rectified Signal Averaging for Fetal Acidemia Identification

Massimo W. Rivolta[1], Marco Biraghi[1], Moira Barbieri[2], Tamara Stampalija[2,3], Roberto Sassi[1]

[1]Dipartimento di Informatica, Università degli Studi di Milano, Milan, Italy
[2]Institute for Maternal and Child Health IRCCS "Burlo Garofolo", Trieste, Italy
[3]Dipartimento di Scienze Mediche, Chirurgiche e della Salute, University of Trieste, Trieste, Italy

Abstract

The Phase-Rectified Signal Averaging (PRSA) technique has been widely investigated for the assessment of fetal well-being during labor, through the analysis of the fetal heart rate (FHR) series. PRSA provides the average acceleration and deceleration capacities of FHR by means of synchronous average of segments associated with either an increase or decrease of the FHR. The identification of which segments to average and the computation of the capacities are currently based on the Haar wavelet at scale T and s, respectively. In this study, we proposed a generalization of the PRSA algorithm by changing the wavelet involved. We tested five different wavelets, i.e., Haar, Shannon, Morlet and two versions of Poisson's, for the identification of acidemia at birth on FHR recordings collected during labor. The ranking of the top five wavelets was created using the area-under-the-curve (AUC) of the ROC analysis. The Haar wavelet was outperformed by Shannon and Poisson wavelets, with an AUC of 0.65 and 0.60, respectively. The findings suggest that different wavelets may be more appropriate for acidemia detection.

1. Introduction

The Phase-Rectified Signal Averaging (PRSA) technique [1] applied to the fetal heart rate FHR (FHR) series has found a wide room of investigation for the assessment of fetal well-being during pregnancy monitoring [2] and labor [3,4]. PRSA provides the average acceleration (AC) and deceleration (DC) capacities of FHR by means of synchronous average of segments associated with either an increase or decrease of the heart rate [1,5].

During labor, its success for fetal surveillance may be due to several factors. Indeed, given the fact that FHR series is usually very noisy and presents FHR decelerations due to maternal contractions, PRSA has several advantages over other techniques (*e.g.*, spectral analysis) in this context. First, PRSA does not require stationary series and can be applied on the entire recording. Second, it tolerates a large amount of missing values due to the high number of segments usually identified for computing the synchronous average. Third, PRSA depends on three parameters (*i.e.*, L, T, and s) that control the frequency band to mostly enhance. Fourth, the average operator reduces the noise over the series and the fact that this average is synchronized to increasing or decreasing trends of FHR makes it anchored to important events such as FHR accelerations and decelerations.

The identification of segments to be averaged is performed by detecting the so-called anchor points. These points are defined as those having the average of T successive samples (including the anchor) of the FHR series greater/lower than the average of T previous ones, *i.e.*, a local FHR acceleration/deceleration. After performing the synchronous average of all FHR segments centered at each anchor point, that produces that PRSA series (a vector of $2L$ elements), AC and DC are computed in a similar fashion on the PRSA series, *i.e.*, the average of s samples after the anchor point subtracted by the average of the previous s ones. This approach assigns equal weights to all samples for anchor point identification and capacity computation.

In this study, we proposed a generalization of the PRSA algorithm by defining a different weight for each sample for the identification of anchor points and computation of capacities. The weights were defined by 4 wavelets. We tested these wavelets and ranked them using the area-under-the-curve (AUC) computed through ROC analysis for the identification of acidemia at birth using cardiotocographic recordings (CTG) collected during labor.

2. Methods

2.1. Background on AC and DC

The PRSA algorithm involves three steps to compute AC and DC from the FHR series: i) identification of the anchor points; ii) synchronous average for computing the

 ISSN: 2325-887X DOI: 10.22489/CinC.2021.180

PRSA series; and iii) computation of AC and DC from the PRSA series.

First, all the time indices t such that

$$\mathcal{A}_{\mathrm{AC}} = \left\{ t : \frac{1}{T}\sum_{i=0}^{T-1} \mathrm{FHR}[t+i] > \frac{1}{T}\sum_{i=1}^{T} \mathrm{FHR}[t-i] \right\} \quad (1)$$

are termed "anchor points". The integer value T sets the "timescale" and the set $\mathcal{A}_{\mathrm{AC}}$ is the "accelerations' list". The "decelerations' list" $\mathcal{A}_{\mathrm{DC}}$ is instead built by changing the direction of the inequality in (1). Second, a window of length $2L$ samples is centered on each anchor point (the anchor point is at position $L+1$). Then, the windows (one for each anchor point) are aligned and averaged synchronously, obtaining the PRSA series of $2L$ samples. Third, the PRSA series is used to compute the capacity with

$$\mathrm{AC} = \frac{1}{2s}\sum_{i=1}^{s} \mathrm{PRSA}[L+i] - \frac{1}{2s}\sum_{i=0}^{s-1} \mathrm{PRSA}[L-i] \quad (2)$$

where s is the scale. DC is computed with the same formula, but with a different PRSA series obtained using the decelerations' list $\mathcal{A}_{\mathrm{DC}}$.

It is worth noting that (1) and (2) are obtained by applying the Haar wavelet at scale T and s, respectively, as pointed out in [1].

2.2. Generalization of the PRSA Algorithm

The algorithm described in sec. (2.1) can be generalized by changing the wavelet family for both anchor point identification and capacity computation. However, depending on the wavelet, this change makes the anchor points anchored on events different from local accelerations and decelerations. Therefore, the terms AC and DC lose sense in this generalization. On the other hand, the use of a different wavelet may optimize the recognition of relevant patterns on the FHR series (*e.g.*, acidemia, sinusoidal pattern).

The generalization works as follows. First, the identification of anchor points becomes

$$\mathcal{A} = \left\{ t : \sum_{i=1}^{2L} w_T[i]\mathrm{FHR}[t-L+i-1] > 0 \right\} \quad (3)$$

where $w_T[i]$ is the i-th sample of the wavelet w at scale T, stored in a vector of $2L$ elements (indexed from 1). Then, the capacity c_s at scale s is computed using

$$c_s = \frac{1}{2s}\sum_{i=1}^{2L} w_s[i]\mathrm{PRSA}[i] \quad (4)$$

where w_s is the same wavelet used for the identification of anchor points but a scale s, whereas PRSA is the synchronous average of windows around anchor points as in (2).

Given the fact the during labor, FHR may present a skewed distribution due to maternal contractions, it make sense to switch the inequality in (3) as well (similarly to the decelerations' list). We refer to these two different lists as $\mathcal{A}_{>}$ and $\mathcal{A}_{<}$ depending on the inequality sign.

2.3. Wavelets

In this study, we tested five different wavelets belonging to four wavelet families, *i.e.*, Haar, Morlet, Shannon and Poisson. It is known that FHR decelerations are slow-varying phenomena ($\approx$ one deceleration every two or three minutes at its peak) and their morphology has diagnostic power. Bearing these considerations in mind, wavelets should be able to enhance the accelerating and decelerating trends during the FHR decelerations and to be sensitive to slow changes in FHR. Haar and Poisson wavelets act as derivative filters, thus enhancing the trends, while Morlet and Shannon wavelets are equivalent to band pass filters, thus they should be sensitive to low frequency components of the FHR series. The cutoff frequencies of these filters are controlled by the scale of the wavelet [6].

In order to use the wavelet selected in the generalized PRSA algorithm, we adapted their mathematical formulation. The adaptation was necessary to have: i) the scale dependent on the parameter a; ii) a bounded wavelet between $[-1,1]$; and iii) the symmetry axis or zero crossing of the wavelet in the anchor point.

The Haar wavelet was defined as follows (as in [1])

$$w_a[i] = \begin{cases} 1 & L+1 \le i \le L+a \\ -1 & L-a+1 \le i \le L \\ 0 & \text{otherwise} \end{cases} \quad (5)$$

The Morlet wavelet was defined as follows

$$w_a[i] = e^{-\left(\frac{i-L-1}{\sqrt{2}a}\right)^2} \cos\left(\frac{\sigma(i-L-1)}{a}\right) \quad (6)$$

where σ controls the scale (similar to a). Here, we set $\sigma = 5$ as commonly used.

The Shannon wavelet was defined as follows

$$w_a[i] = \mathrm{sinc}\left(\frac{i-L-1}{2a}\right) \cos\left(\frac{3\pi(i-L-1)}{2a}\right) \quad (7)$$

Two versions of the Poisson wavelet were built by means of the two following steps. First, we defined the function

$$f_{a,n}[i] = \begin{cases} \left(\frac{\frac{i+an}{a}-n}{n!}\right)\left(\frac{i+an}{a}\right)^{n-1} e^{-\frac{i+an}{a}} & i \ge -an \\ 0 & \text{otherwise} \end{cases} \quad (8)$$

where n is a parameter of the Poisson wavelet. The function f is a shifted version of the Poisson wavelet in such a way that the function is 0 at $i = -an$.

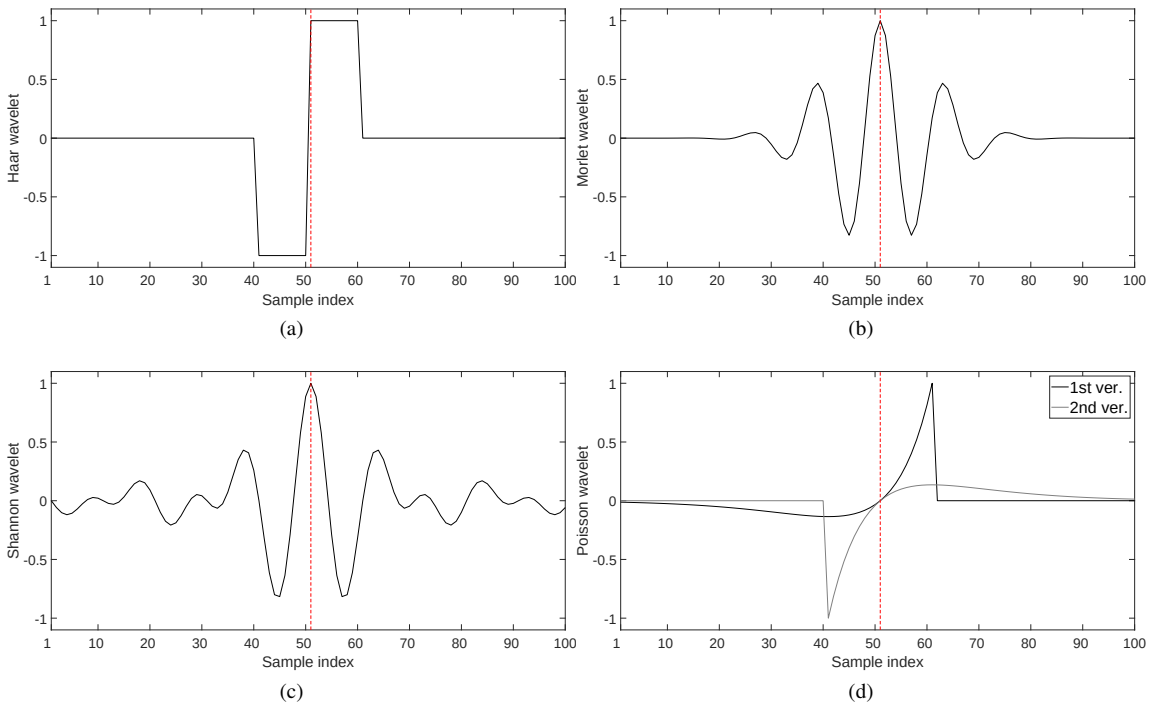

Figure 1: Example of five wavelets with $a = 10$ and $L = 50$ for all panels: Haar's (a), Morlet's (b), Shannon's (c) and two versions of Poisson's (d). The red dashed lines represent the position of the anchor point in the wavelet (*i.e.*, $L + 1$).

Then, the first version was defined as follows

$$w_a[i] = -\frac{f_{a,n}[-(i - L - 1)]}{\max\{|f_{a,n}[a\sqrt{n}]|, |f_{a,n}[-a\sqrt{n}]|\}} \quad (9)$$

while the second one was

$$w_a[i] = \frac{f_{a,n}[i - L - 1]}{\max\{|f_{a,n}[a\sqrt{n}]|, |f_{a,n}[-a\sqrt{n}]|\}} \quad (10)$$

The denominator of (9) and (10) rescaled the wavelets in the range $[-1, 1]$. Here, we used $n = 1$. The rationale behind the definition of two Poisson wavelets was the asymmetric behavior of its original formulation. Indeed, the function f weights the samples after the anchor point differently from those before, making past or future samples play a different role in the PRSA algorithm.

Figure 1 shows an example for each wavelet.

2.4. Database and CTG Preprocessing

The CTU-UHB Intrapartum Cardiotocography Database from Physionet [7, 8] was used to test the capacity c on human data. It contains carefully selected CTG recordings of 552 fetuses (singleton, uncomplicated pregnancies, with no congenital defects and week of gestation $\geq$ 37) resampled at 4 Hz (for further details, please refer to [7]). Umbilical artery pH was also available for each fetus at birth. Forty-four fetuses had an umbilical artery pH value ≤ 7.05 and, in this study, were considered as acidotic.

CTG recordings were analyzed during the last hour before stage II of the labor. Missing beats were linearly interpolated and the reconstructed samples were not allowed to be anchor points. In addition, only series with less than 30% of missing beats were further considered. Overall, 24 acidotic and 441 healthy fetuses were analyzed. The preprocessing was the same performed in [9].

2.5. Experiments

We computed the capacities for all wavelets using the following configurations: i) $T = 1$ and $s = 2$ [9]; ii) $T = 5$ and $s = 5$ [3]; and iii) $T = 10$ and $s = 10$ [4]. Both $\mathcal{A}_>$ and $\mathcal{A}_<$ were considered. These configurations were found as relevant for acidemia detection in the cited studies.

A ROC analysis was performed for all capacities extracted to detect acidemia at birth. The AUC was used to build the ranking of wavelets. The five highest average AUC values are reported. Bootstrapping with 2000 iterations was applied to estimate the 90% confidence interval (CI) of the AUC estimates for each configuration (as done in [4]).

Table 1: Average and 90% CI of AUC for the top five wavelets, along with the corresponding configuration of T and s.

	$\mathcal{A}_>$				$\mathcal{A}_<$			
Ranking	Wavelet	T	s	AUC	Wavelet	T	s	AUC
1	Shannon	5	5	0.65 (0.55, 0.75)	Poisson 2nd ver.	10	10	0.60 (0.51, 0.70)
2	Shannon	10	10	0.60 (0.50, 0.71)	Haar	1	2	0.58 (0.48, 0.70)
3	Poisson 1st ver.	10	10	0.59 (0.49, 0.69)	Shannon	10	10	0.57 (0.47, 0.67)
4	Poisson 2nd ver.	5	5	0.58 (0.48, 0.69)	Poisson 2nd ver.	5	5	0.57 (0.47, 0.67)
5	Haar	1	2	0.57 (0.48, 0.67)	Poisson 2nd ver.	1	2	0.56 (0.46, 0.66)

3. Results

Table 1 reports the average and confidence interval of AUC for the top five wavelets, along with the corresponding configuration of T and s. The average AUC of the top five wavelets ranged between 0.56 and 0.65. The two top performing wavelets were the Shannon's one with $T = 5$ and $s = 5$ for $\mathcal{A}_>$ (0.65) and the second version of Poisson wavelet for $\mathcal{A}_<$ (0.60). The Haar wavelet ranked fifth in acceleration mode (0.57) and second in deceleration (0.58).

Among the five selected wavelets, the second version of Poisson wavelet appeared in the ranking four times (the highest) while the Morlet's did not appear in the top five.

4. Discussions

In this study, we proposed a generalization of the PRSA algorithm by changing the wavelet used for the identification of anchor points and computation of the capacity. In addition, we tested five different wavelets for the identification of acidemia at birth using CTG recordings collected during labor. The range of AUC was similar to the one in Georgieva *et al.*'s study, which reported an AUC of 0.67 for detecting pH $\leq$ 7.05 on a dataset of more than 7000 pregnancies [3]. They analyzed CTG recordings and found the best combination of T and s values between 5 and 10. Interestingly, the Haar wavelet at this configuration did not appear in the top five performers. A possible explanation could be that, in their study, they analyzed the stage II of labor, where more FHR decelerations are present.

Differently from the Haar wavelet, the others were not symmetric with respect to the x-axis (Fig. 1). From one hand, such asymmetry have played an important role in the identification of acidemia, as shown in Table 1. On the other hand, it made the identification of anchor points more challenging, especially for low values of scale T. For example, no anchor points were found in $\mathcal{A}_<$ with $T = 1$ for the Shannon wavelet.

Further analyses are necessary to assess the limits of the proposed generalization.

References

[1] Bauer A, Kantelhardt JW, Bunde A, Barthel P, Schneider R, et al. Phase-rectified signal averaging detects quasi-periodicities in non-stationary data. Physica A 2006; 364:423–434.

[2] Stampalija T, Casati D, Montico M, Sassi R, Rivolta MW, Maggi V, Bauer A, Ferrazzi E. Parameters influence on acceleration and deceleration capacity based on trans-abdominal ECG in early fetal growth restriction at different gestational age epochs. Eur J Obstet Gynecol Reprod Biol 2015;188:104–112. ISSN 03012115.

[3] Georgieva A, Papageorghiou AT, Payne SJ, Moulden M, Redman CWG. Phase-rectified signal averaging for intrapartum electronic fetal heart rate monitoring is related to acidaemia at birth. BJOG 2014;121(7):889–894.

[4] Lobmaier SM, Mensing van Charante N, Ferrazzi E, et al. Phase-rectified signal averaging method to predict perinatal outcome in infants with very preterm fetal growth restriction-a secondary analysis of TRUFFLE-trial. Am J Obstet Gynecol 2016;215:630.e1–7.

[5] Kantelhardt JW, Bauer A, Schumann AY, Barthel P, Schneider R, et al. Phase-rectified signal averaging for the detection of quasi-periodicities and the prediction of cardiovascular risk. Chaos Interdiscip J Nonlinear Sci 2007;17:015112.

[6] Sassi R, Stampalija T, Casati D, Ferrazzi E, Bauer A, et al. A methodological assessment of phase-rectified signal averaging through simulated beat-to-beat interval time series. Comput Cardiol 2014;41:601–604.

[7] Chudáček V, Spilka J, Burša M, Janků P, Hruban L, et al. Open access intrapartum CTG database. BMC Pregnancy Childbirth 2014;14:16.

[8] Goldberger AL, Amaral LAN, Glass L, Hausdorff JM, Ivanov PC, et al. PhysioBank, PhysioToolkit, and PhysioNet: Components of a new research resource for complex physiologic signals. Circulation 2000;101:e215–e220.

[9] Rivolta MW, Stampalija T, Frasch MG, Sassi R. Theoretical value of deceleration capacity points to deceleration reserve of fetal heart rate. IEEE Trans Biomed Eng 2020; 67(4):1176–1185.

Address for correspondence:

Massimo W. Rivolta
Dipartimento di Informatica, Università degli Studi di Milano, Via Celoria 18, 20133, Milan, Italy
massimo.rivolta@unimi.it